New Journal of Physics
The open access journal at the forefront of physics

Deutsche Physikalische Gesellschaft DPG IOP Institute of Physics

PAPER • OPEN ACCESS

Time-domain optics for atomic quantum matter

To cite this article: Simon Kanthak *et al* 2021 *New J. Phys.* **23** 093002

New Journal of Physics
The open access journal at the forefront of physics

Deutsche Physikalische Gesellschaft DPG
IOP Institute of Physics

Published in partnership with: Deutsche Physikalische Gesellschaft and the Institute of Physics

OPEN ACCESS

RECEIVED
15 May 2021

ACCEPTED FOR PUBLICATION
8 July 2021

PUBLISHED
1 September 2021

PAPER

Time-domain optics for atomic quantum matter

Simon Kanthak[1,2,*], Martina Gebbe[3], Matthias Gersemann[4], Sven Abend[4], Ernst M Rasel[4] and Markus Krutzik[1,2]

[1] Institut für Physik, Humboldt-Universität zu Berlin, Newtonstraße 15, 12489, Berlin, Germany
[2] Joint Lab Integrated Quantum Sensors, Ferdinand-Braun-Institut gGmbH, Leibniz-Institut für Höchstfrequenztechnik, Gustav-Kirchhoff-Straße 4, 12489 Berlin, Germany
[3] Zentrum für Angewandte Raumfahrt und Mikrogravitation (ZARM), Universität Bremen, Am Fallturm 2, 28359 Bremen, Germany
[4] Institut für Quantenoptik, Leibniz Universität Hannover, Welfengarten 1, 30167 Hannover, Germany
[*] Author to whom any correspondence should be addressed.

E-mail: kanthak@physik.hu-berlin.de

Keywords: Bose–Einstein condensates, ultra-cold atoms, matter-wave lensing, time-domain optics, optical dipole traps, atom-chip traps, matter-wave telescope

Abstract

We investigate time-domain optics for atomic quantum matter. Within a matter-wave analog of the thin-lens formalism, we study optical lenses of different shapes and refractive powers to precisely control the dispersion of Bose–Einstein condensates. Anharmonicities of the lensing potential are incorporated in the formalism with a decomposition of the center-of-mass motion and expansion of the atoms, allowing to probe the lensing potential with micrometer resolution. By arranging two lenses in time formed by the potentials of an optical dipole trap and an atom-chip trap, we realize a magneto-optical matter-wave telescope. We employ this hybrid telescope to manipulate the expansion and aspect ratio of the ensembles. The experimental results are compared to numerical simulations that involve Gaussian shaped potentials to accommodate lens shapes beyond the harmonic approximation.

1. Introduction

Various concepts of photonics can be applied to atomic matter waves by exploiting the dissipative and the dispersive interactions of atoms with external fields [1, 2]. Following electron and neutron optics [3, 4], lenses for atomic de Broglie waves based on magnetic [5, 6] and optical potentials [7–9] are employed in atomic waveguides [10, 11] and in free fall [12, 13] to converge [14], collimate [15] or diverge [16] atomic ensembles.

In this paper, we utilize a single beam optical dipole trap (ODT) to form various types of matter-wave lenses applied to Bose–Einstein condensates (BECs). We tune the shape and the refractive power of the atom lens through timing, power and duration of the optical pulses following a time-domain analog of the thin-lens formalism [17, 18]. Thanks to the single-mode properties and small spatial extents of BECs, we can probe the lensing potential with a spatial resolution of the order of microns. By arranging two lenses in time formed by the potentials of an ODT and an atom-chip trap, we then realize a magneto-optical matter-wave telescope to precisely control the expansion and aspect ratio of atomic quantum matter.

Due to their point-source like characteristics, BECs constitute ideal quantum probes to study precision atom optics and feature important properties for application in interferometry such as small spatial extension, low expansion velocities and large spatial coherence. BECs are proposed for application or already employed in gravimeters [19–21] and tiltmeters [10, 22], magnetometers and magnetic gradiometers [23, 24] and gyroscopes [25]. Aiming at high inertial sensitivities using extended interferometer times requires exquisite control over the atomic motion, in particular the wave packet's expansion. The latter is determined by the features of the release trap and, unlike photonic waves, is modified by density-dependent atom-atom interactions. This brings the need for, e.g. dilute ensembles [26], control of the atomic interactions [27], optimized release protocols [28], or shaping of the atomic expansions after release from the trapping potential e.g. by delta-kick collimation (DKC) [29]. Collimation

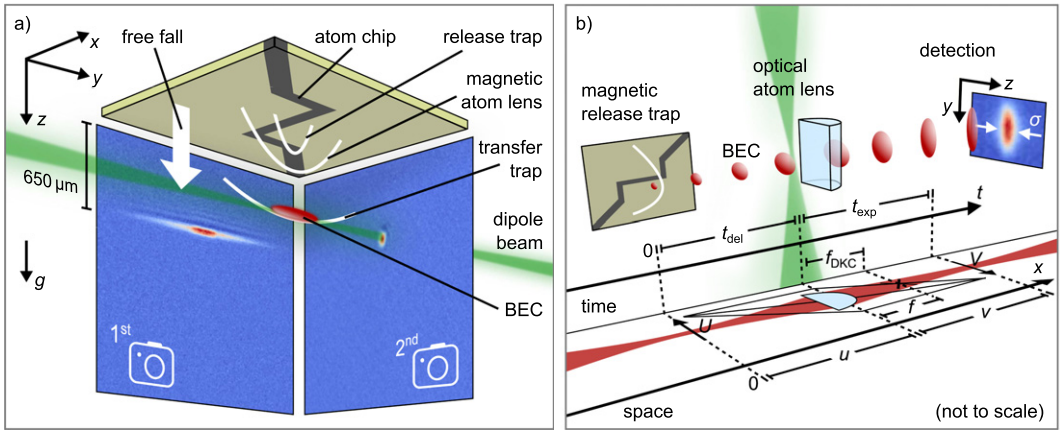

Figure 1. Matter-wave lensing of chip-based BECs. (a) The hybrid setup for matter-wave lensing is formed by an ODT at 1064 nm (green single beam) below the surface of an atom chip (beige layer with dark gray wire), which allows for the creation of different magnetic potentials (white parabolas). After preparation within the atom-chip trap, the BEC is released into free fall for matter-wave lensing with optical and magnetic potentials. Two absorption imaging axes allow for the observation of the BEC along and perpendicular to the dipole beam. (b) Illustration of time-domain optics with an optical atom lens. The image formation can be predicted within a matter-wave analog of the thin-lens formalism, see equations (4) and (5).

of atomic matter waves resulting in ultra-narrow velocity distributions already enables macroscopic interferometer times [12, 13, 30], efficient transfers of large momentum [10, 31], and observation of the long-time evolution of matter waves [32, 33]. However, full flexibility and control over dispersion and size of atomic ensembles require matter-wave lenses of various shapes and refractive powers. Towards this end, single lenses or optical lens systems have to be precisely engineered in time series by tailored potentials, while the matter-wave packets expand in free space, and anharmonicites of the conservative potentials need to be taken into account.

The paper is structured as follows: section 2 introduces our combined atom-chip and dipole trap setup and describes the experimental sequence for matter-wave lensing. In section 3, we present the numerical method used to describe the evolution of BECs after release and manipulation in optical potentials. We show results on matter-wave optics with our optical lenses and a hybrid matter-wave telescope. In section 4 we give a conclusion of the results and discuss limitations of the presented methods.

2. Experimental setup and sequence

2.1. Matter-wave lensing of chip-based BECs

Our atom-optics experiments are based on a hybrid atom trap consisting of a magnetic atom-chip trap and a single beam ODT, as illustrated in figure 1(a). This geometry is implemented in the BEC apparatus which is described in detail in [12, 34]. The experiment's atom chip typically generates BECs of up to 1.5×10^4 ^{87}Rb atoms in the magnetic $|F = 2, m_F = 2\rangle$ state within 12 s of repetition time. The apparatus allows for the creation of magnetic traps of various trap frequencies connected to different distances below the chip surface, where the potential of a far-detuned Gaussian beam enables optical trapping and matter-wave lensing. Both the magnetic trap and the ODT are ellipsoid in shape and their principal axes are perpendicular to each other.

Figure 1(b) shows the experimental sequence for optical matter-wave lensing. After release from a magnetic trap (named release trap) centered above the optical beam, the BEC drops and freely expands for a delay time t_{del} until we apply a temporally shaped, Gaussian pulse of the dipole beam ($1/e^2$ width τ). An absorption image is taken after a total expansion time t, from which we determine the center-of-mass (COM) position Δ and size σ of the ensemble with Gaussian fits to the atomic density distribution. Table 1 shows the release trap's frequencies ($\omega_\xi, \xi \in \{x, y, z\}$) and center position ($\Delta_{z,0}$, measured from the chip surface) together with the initial BEC size ($\sigma_{z,0}$). In addition, we include the parameters of an optical and a magnetic matter-wave lens.

2.2. An optical matter-wave lens in the vicinity of an atom chip

As a light source for the optical matter-wave lens, we use a high-power fiber amplifier system [NKT Photonics, Boostik] with a low-noise, single-frequency laser [NKT Photonics, Koheras

Table 1. Parameters of the employed optical and magnetic potentials. Trap features of the magnetic trap used to release a BEC for matter-wave lensing alongside the two lensing potentials which form our hybrid matter-wave telescope. We indicate the shape of the lenses in each dimension with a convex lens for $\omega_{\mathrm{DKC}} \in \mathrm{Re}$ and a concave lens for $\omega_{\mathrm{DKC}} \in \mathrm{Im}$. The COM position $\Delta_{z,0}$ refers to the surface of the atom chip. The initial sizes of the BEC in the other dimensions are given by $\sigma_{\xi,0}\sqrt{\omega_\xi} = \sigma_{\zeta,0}\sqrt{\omega_\zeta}$.

	$\omega_x(2\pi\cdot\mathrm{Hz})$	$\omega_y(2\pi\cdot\mathrm{Hz})$	$\omega_z(2\pi\cdot\mathrm{Hz})$	$\Delta_{z,0}\,(\mu\mathrm{m})$	$\sigma_{z,0}\,(\mu\mathrm{m})$
release trap	18	131	127	395	1.3
magnetic lens	44 → convex	113 → convex	$90i$ → concave	570	-
optical lens	240 → convex	3 → flat	240 → convex	650	-

Adjustik] emitting linearly polarized light at 1064 nm with an FWHM linewidth of 3 kHz. The emitted light is amplified by a fiber amplifier, which provides up to 10 W of optical output power[5].

The amplifier's output is delivered to an optical distribution system for optical pulse shaping. The light passes through an optical isolator [Thorlabs, IO-5-1064-VHP], before the power is dynamically adjusted by an acousto-optical modulator [AA Opto-Electronics, MTS80-A3-1064Ac] driven by radio-frequency pulses from an arbitrary waveform generator. A mechanical shutter [NM Laser, LST400] is used to fully block the light to avoid disturbance of the BEC generation. The light is fiber-coupled and guided to the ultra-high vacuum (UHV) chamber via a polarization-maintaining single-mode fiber.

At the exit port of the single-mode fiber, a triplet-lens fiber collimator [Thorlabs, TC25FC-1064] creates a Gaussian-shaped beam. A single lens ($f = 200$ mm) focuses the light to a $1/e^2$ waist of $w_0 = 33\ \mu$m located 650 μm below the atom chip. With a 60 mW single Gaussian beam, we realize an optical potential with trap frequencies of $\omega_{\mathrm{radial}} = 2\pi \cdot 230$ Hz and $\omega_{\mathrm{axial}} = 2\pi \cdot 2$ Hz along the radial and axial axes respectively, and with trap depth of $\hat{U} = k_{\mathrm{B}} \cdot 5\ \mu$K for ^{87}Rb atoms. The dipole beam is leveled with respect to gravity and a photodiode at the backside of the chamber monitors its optical power.

Absorption images of the atomic ensembles can be taken from two orthogonal directions: parallel and perpendicular to the dipole beam, as shown in figure 1(a). The imaging beam along the propagation of the dipole beam is coupled through the chamber via two dichroic mirrors in front of and behind the UHV chamber, whereas the perpendicular imaging beam enters via a window from the side.

3. Methods and results

3.1. Scaling approach with a Gaussian shaped potential

We predict the dynamics of a BEC through a variational ansatz to numerically solve the time-dependent Gross–Pitaevskii equation following a scaling approach [35, 36]. As trial functions, we choose a Gaussian ansatz of the form

$$\psi(x,y,z,t) = \sqrt{\frac{N_0}{(2\pi)^{\frac{3}{2}}}} \prod_{\xi\in\{x,y,z\}} \frac{1}{\sqrt{\sigma_\xi}} \exp\left[-\frac{(\xi-\Delta_\xi)^2}{4\sigma_\xi^2} + \mathrm{i}\alpha_\xi\xi + \mathrm{i}\beta_\xi\xi^2\right], \tag{1}$$

where Δ_ξ is the COM position, σ_ξ is the size of the BEC, α_ξ accounts for the COM kinetic energy, and β_ξ is proportional to the inverse square root of the radius of curvature for a BEC of atom number N_0. The evolution equations for these parameters are obtained by solving the Lagrange equations

$$\frac{\partial L(\psi,\psi^\dagger)}{\partial q_\xi} - \frac{\mathrm{d}}{\mathrm{d}t}\frac{\partial L(\psi,\psi^\dagger)}{\partial \dot{q}_\xi} = 0, \quad q_\xi(t) \in \{\Delta_\xi, \sigma_\xi, \alpha_\xi, \beta_\xi\}(t). \tag{2}$$

We model the optical atom lens with a 3D Gaussian potential instead of a harmonic approximation [36] given by

$$U_{\mathrm{dip}}(x,y,z,t) = -\hat{U}(P)\exp\left[-\frac{(t-t_{\mathrm{del}})^2}{2\tau^2}\right] \prod_{\xi\in\{x,y,z\}} \exp\left[-2\frac{\xi^2}{w_{0,\xi}^2}\right], \tag{3}$$

where the trap depth is a function of optical power $\hat{U}(P) = k_{\mathrm{B}} \cdot 5\ \mu\mathrm{K}/60\ \mathrm{mW} \cdot P$ for a single dipole beam with $1/e^2$ waists of $w_{0,x} = w_{0,z} = 33\ \mu$m (radial axes) and Rayleigh range $y_{\mathrm{R}} = 3.2$ mm $\approx w_{0,y}/\sqrt{2}$ (axial axis)[6]. For matter-wave lensing, we define a time-dependent, Gaussian envelope $h(t)$ of width τ delayed by

[5] Less than 600 mW of optical power are used for the presented work.
[6] We assume $w_{0,\xi} \gg \sigma_\xi$ in the evolution equations (parabolic lens).

t_{del} after the release of the BEC. The initial values $q_\xi(t = 0\ \mathrm{s}) = q_{\xi,0}$ for the numerical simulations are determined by matching the trajectories of the BECs and their asymptotic expansions with the experimental data obtained from time-of-flight (ToF) measurements. The initial positions $\Delta_{z,0}$ and size $\sigma_{z,0}$ for the atom-chip trap are shown in table 1. Sizes in the other dimensions are given by $\sigma_{\xi,0}\sqrt{\omega_\xi} = \sigma_{\zeta,0}\sqrt{\omega_\zeta}$.

3.2. Thin-lens formalism for matter waves

Matter waves subjected to an atom lens underly an isomorph formalism analog to the description of photonic waves passing a thin lens [17, 18], as illustrated in figure 1(b),

$$\frac{1}{u} + \frac{1}{v} = \frac{1}{f} \quad \Leftrightarrow \quad \frac{1}{t_{\mathrm{del}}} + \frac{1}{t_{\mathrm{exp}}} = \frac{1}{f_{\mathrm{DKC}}}, \tag{4}$$

$$\pm\frac{V}{U} = \frac{v}{f} - 1 \quad \Leftrightarrow \quad \pm\frac{\sigma}{\sigma_0} = \frac{t_{\mathrm{exp}}}{f_{\mathrm{DKC}}} - 1, \tag{5}$$

where (u, t_{del}) is the distance from the object to the lens and (v, t_{exp}) is the distance from the lens to the image, respectively in space and time. (U, σ_0) is the size of the object and (V, σ) is the size of the image. Location and magnification depend on the refractive power of the lens, which inversely relates to a focal length f for photonic waves and a focal time f_{DKC} for time-domain optics with matter waves.

A matter-wave lens is achieved e.g. by switching on an optical potential of trap frequency ω_{DKC}, and can be approximated by a thin lens

$$f_{\mathrm{DKC}}^{-1}(P, \tau, t_{\mathrm{del}}) = \int_{-\infty}^{+\infty} \omega_{\mathrm{DKC}}^2(P, t) \cdot h(t)\mathrm{d}t \approx \omega_{\mathrm{DKC}}^2(P, t_{\mathrm{del}}) \cdot \tau\sqrt{2\pi}, \tag{6}$$

if the pulse is relatively short such that $\omega_{\mathrm{DKC}}(t_{\mathrm{del}} \pm \tau) \approx \omega_{\mathrm{DKC}}(t_{\mathrm{del}})$. Such a lens can ultimately be used to control the dispersion of matter waves. Like in photonics, a convex lens with $f_{\mathrm{DKC}} > 0$ converges, while a concave lens with $f_{\mathrm{DKC}} < 0$ diverges matter waves. Thus ω_{DKC} is a complex quantity in this formalism which we therefore refer to as an effective trap frequency.

3.3. Characterization of the optical matter-wave lens

Control of the dispersion and size of atomic ensembles requires a careful adjustment of the refractive power of the matter-wave lens and, hence, an analysis of the lensing potentials. For this purpose, we either examine the magnification of lensed matter waves or directly measure the trap frequencies of the lensing potential.

First, we determine the trap frequencies of our optical matter-wave lens from collective-mode oscillations inside the dipole potential. For transfer into the ODT, we prepare a BEC in the magnetic trap (named transfer trap) whose trap center is spatially overlapped with the dipole beam, as shown in figure 1(a). We linearly ramp up the optical power to $P = 60$ mW within 50 ms and, after temporal overlap of the two traps for additional 50 ms, we switch off the magnetic fields. Subsequently, we observe size oscillations with a period of 416 ms along the axial direction of the dipole beam, caused by the non-adiabatic decompression of the trap frequencies from the atom-chip trap ($\omega_y = 2\pi\cdot$ 46 Hz) to the ODT ($\omega_y = 2\pi\cdot$ 2 Hz), as shown in figure 2(a).[7] Residual spatial displacements of $\Delta_{x,0} = 2\ \mu$m and $\Delta_{z,0} = 21\ \mu$m of the traps lead to COM oscillations along the radial directions of the beam with periods of 4 ms and $1/e$ dampings of $\Gamma_x = 31\ \mathrm{s}^{-1}$ and $\Gamma_z = 101\ \mathrm{s}^{-1}$, as shown in figure 2(b). We obtain the initial displacement, trap frequencies, damping coefficients, and phase of the COM oscillations from the experimental data (symbols) with fits (lines) of the form $\Delta_\xi(t) = \Delta_{\xi,0}\ \sin\left(\omega_\xi t + \Phi_\xi\right) \cdot \exp\left(-\Gamma_\xi t\right)$. The resulting trap frequencies of the optical potential are $\omega_{x,y,z} = 2\pi \cdot (230, 2, 228)$ Hz.

Second, we utilize the magnification of the matter waves as a measure of the lensing potential. According to equation (5), the magnification is inversely proportional to the focal time of the matter-wave lens and a modification for arbitrary expansion times together with equation (6) reads

$$\frac{\sigma'(t) \pm \sigma(t)}{\sigma'(t_{\mathrm{del}})} = (t - t_{\mathrm{del}}) \cdot \omega_{\mathrm{DKC}}^2(P, t_{\mathrm{del}}) \cdot \tau\sqrt{2\pi}, \tag{7}$$

where the prime distinguishes between the freely propagating (σ') and the lensed BEC (σ). With σ' determined by the release trap itself, the effective trap frequency ω_{DKC} of the matter-wave lens is accessible by measuring $\sigma(t)$.

Figure 2(c) shows trap frequencies of matter-wave lenses for various optical powers ranging from 0 to 600 mW. The delay time and duration of the optical pulses are $t_{\mathrm{del}} = 7.2$ ms and $\tau = 6.3\ \mu$s. Trap

[7] We obtain the size of the condensate fraction inside the ODT from bimodal fits to the atomic density distribution to account for atoms inside the thermal background.

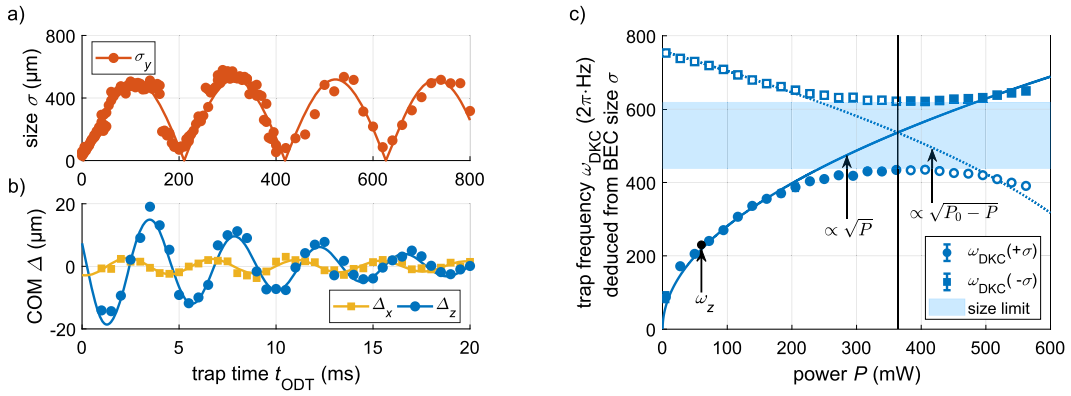

Figure 2. Characterization of the optical matter-wave lens. (a) Size and (b) COM oscillations of the BEC after transfer from the atom-chip trap into an ODT of 60 mW optical power. The lines denote fits from where we obtain the trap frequencies $\omega_{x,y,z} = 2\pi \cdot (230, 2, 228)$ Hz of the lensing potential. (c) Trap frequencies derived from the magnification of matter-waves in dependence of power of the optical pulses. The experimental data (symbols) is deduced from the size of lensed ensembles after a total expansion time of $t = 33.4$ ms. The delay time and duration of the optical pulses are $t_{del} = 7.2$ ms and $\tau = 6.3$ μs. From equation (7), two branches arise that correspond to lensed matter waves detected before (circles) and after (squares) occurrence of a focus. Analytical expressions based on the standard power low of a single beam ODT are shown as lines. Deviations result from the minimum observable and minimum achievable size in the experiment (shaded area) due to aberrations of the matter-wave lens and the detection limit. We include ω_z obtained from the COM oscillations in (b).

frequencies (symbols) are experimentally derived from the size of lensed ensembles after a total expansion time of $t = 33.4$ ms. Analytical expressions of equation (7) using the standard power law of a single beam ODT are shown as lines. Two branches $\omega_{DKC}(\pm\sigma)$ arise that correspond to lensed matter waves detected before (circles) and after (squares) occurrence of a focus. Their intersection (vertical line) indicates the lens with $\omega_{DKC}(\sigma = 0)$, which causes the matter wave to focus during the detection. From there, we exclude the non-physical parts of the branches $\propto\sqrt{P_0 - P}$ (unfilled symbols and dotted line) from the part obeying the theoretical expectation $\propto\sqrt{P}$ (filled symbols and solid line). For comparison, we include the trap frequency ω_z obtained from the data shown in figure 2(b).

For the experimental data, the two branches do not intersect and are separated by a gap (shaded area). This gap results from a combination of Gross–Pitaevskii interactions at high densities, atoms in the thermal background, lens aberrations of our optical matter-wave lens and aberrations of our imaging system, which limit the minimum achievable and the minimum observable sizes in the experiment, respectively [13]. We refer to this in the following as finite size limit σ_{min}. For sizes $\sigma > \sigma_{min}$, both branches approach the theoretical expectation and we find agreement with the result obtained from collective-mode oscillations. In this way, equation (7) provides a reliable method to measure trap frequencies in the experiment.

3.4. Engineering of concave and convex lenses from a Gaussian beam

Full flexibility in control of the dispersion and size of atomic ensembles requires matter-wave lenses of various shapes to form multiple-lens systems and matter-wave telescopes with lenses precisely arranged in time. For this, we control the shape of our matter-wave lens by carefully matching the COM position of the BEC with the desired location within the lensing potential. According to equation (6), a convex lens ($f_{DKC} > 0$) is achieved if ω_{DKC} is real, and a concave lens ($f_{DKC} < 0$) is achieved if ω_{DKC} becomes imaginary. To this end, we study the impact imposed by the finite trapping volume and anharmonic potential of the Gaussian beam on the matter-wave lens.

With the atoms in free fall, the dipole potential is not stationary within the atom frame and can be Taylor expanded around the COM position of the BEC

$$U_{dip}(z,t) = U_0(t) + F_{dip}(t) \cdot (z - \Delta) + \frac{1}{2} m \cdot \omega_{DKC}^2(t) \cdot (z - \Delta)^2 + \mathcal{O}\left(z^3\right) \tag{8}$$

with time-dependent expansion coefficients U_0 (trap depth), F_{dip} (dipole force acting on the COM position) and ω_{DKC} (effective trap frequencies) taking into account arbitrary anharmonicities of the potential. For the 1D variation of the dipole potential in equation (3), these coefficients are given as

$$U_0(t) = U_{dip}(z,t)\big|_{z=\Delta} = -\hat{U} \exp\left[-2\frac{\Delta^2(t)}{w_0^2}\right] \cdot h(t), \tag{9}$$

$$F_{dip}(t) = \frac{\partial}{\partial z} U_{dip}(z,t)\bigg|_{z=\Delta} = \frac{4U_0(t)}{w_0^2} \cdot \Delta(t), \tag{10}$$

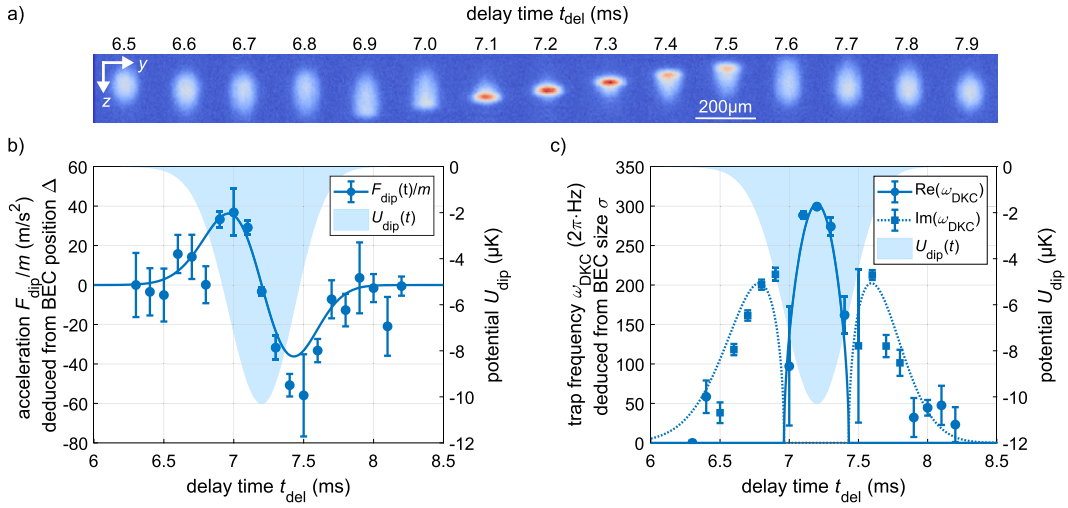

Figure 3. Engineering of concave and convex lenses from a Gaussian beam. (a) Each absorption image shows a BEC after exposure to matter-wave lenses with various delay times between the release from the atom-chip trap and the optical pulse. Power and duration of the pulses are constant with $P = 116$ mW and $\tau = 12.5$ μs. The total expansion time is $t = 33.4$ ms. We obtain the dipole force F_{dip} and effective trap frequencies ω_{DKC} from the COM position Δ and size σ of the lensed ensembles, respectively. (b) Dipole force deduced from experimental data (circles) together with theoretical expectation (line) based on the potential's gradient, equation (10). (c) Effective trap frequencies deduced from experimental data (symbols) together with theoretical expectations (lines) based on the potential's curvature, equation (11). As a consequence of sign change in curvature, the optical lens is convex for $\omega_{DKC} \in$ Re (circles and solid line) and concave for $\omega_{DKC} \in$ Im (squares and dotted line). The shaded areas in (b) and (c) indicate the dipole potential in time domain.

$$\omega_{DKC}(t) = \sqrt{\frac{1}{m}\frac{\partial^2}{\partial z^2}U_{dip}(z,t)\Big|_{z=\Delta}} = \sqrt{\frac{4U_0(t)}{mw_0^2}\left(4\frac{\Delta^2(t)}{w_0^2} - 1\right)}, \tag{11}$$

where $\Delta(t) = \Delta_{z,0} - \frac{1}{2}gt^2$ is the COM position of the atoms, $h(t)$ the time-dependent envelope of the laser pulse and m the particle mass of ^{87}Rb.

We examine the dipole force and effective trap frequency of our matter-wave lens for various delay times t_{del} between the release of the BEC from the atom-chip trap and the optical pulse, as shown in figure 3. Power and duration of the pulses are kept constant with $P = 116$ mW and $\tau = 12.5$ μs. Figure 3(a) shows absorption images taken after a total expansion time of $t = 33.4$ ms while scanning t_{del} from 6.5 to 7.9 ms. We deduce the dipole force and trap frequencies from the COM position and size of the BEC and plot them in figures 3(b) and (c) together with the analytical expressions derived in equations (10) and (11), respectively. For reference, we indicate the dipole potential in time domain as shaded areas.

The experimental data of the dipole force F_{dip} (circles) resolves the shape of the potential's gradient (line), as shown in figure 3(b). At $t_{del} = 7.2$ ms, the trajectory of the BEC $\Delta(t_{del}) = 0$ intersects with the Gaussian beam, where F_{dip} has a zero crossing. Apart from this, the matter waves are suspended to a force during the lens acting on the COM of the BEC, which reaches its extreme values of $\frac{F_{dip}}{m} = \pm\sqrt{2}\frac{4\hat{U}}{mw_0}$ $\approx \pm 40$ m s^{-2} when $\Delta^2(t_{del}) = \frac{w_0^2}{4}$ and drops again to zero when the optical pulse misses the BEC.

The experimental data of the trap frequencies ω_{DKC} (symbols) inherits the shape of the potential's curvature (lines), as shown in figure 3(c). The curvature changes sign, and, as a consequence, $\omega_{DKC} \in$ Re for $\Delta^2(t_{del}) < \frac{w_0^2}{4}$ (circles and solid line) and $\omega_{DKC} \in$ Im for $\Delta^2(t_{del}) > \frac{w_0^2}{4}$ (squares and dotted line). The curvature has an extreme value at the center of the Gaussian beam ($t_{del} = 7.2$ ms), where the effective trap frequency of the lens becomes identical with the harmonic approximation $\omega_{DKC} = \sqrt{\frac{4\hat{U}}{mw_0^2}} \approx 2\pi \cdot 305$ Hz.

With ω_{DKC} time-dependent, we control the focal time's magnitude and sign of our matter-wave lens via the timing of the optical pulses. Depending on the selected delay time, we achieve a convex lens to converge, and a concave lens to diverge matter waves. For any imperfect overlap of the dipole beam and BEC, a COM kick happens, as can be clearly seen in the absorption images in figure 3(a). We note, that the matter-wave lens is subjected to larger shot-to-shot instabilities close to the sign change in focal time, where operation is not desirable.

3.5. Time-domain optics with optical matter-wave lenses

Once the shape of our matter-wave lens is selected with the timing, we further control its focal time through the power and duration of the optical pulses. Here, we demonstrate matter-wave optics with optical lenses

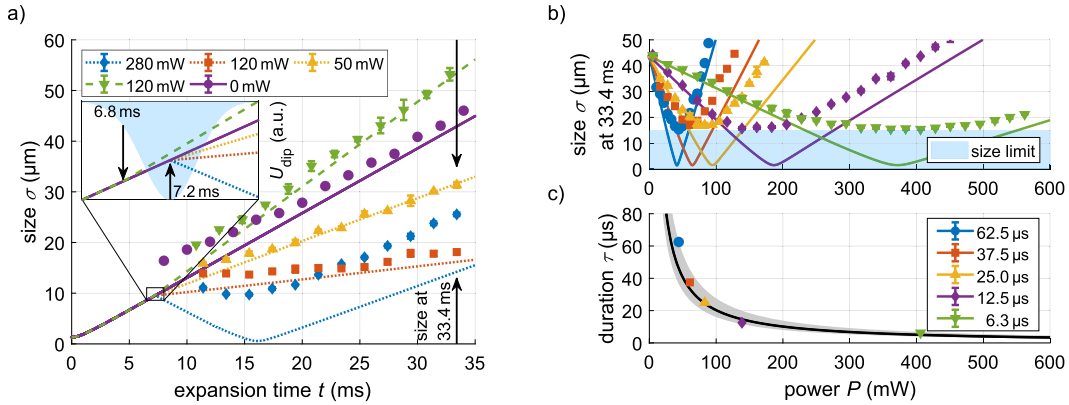

Figure 4. Time-domain optics with optical matter-wave lenses of different shapes and refractive powers. (a) ToF measurements: convex matter-wave lenses (dotted lines) of various optical powers allow to reduce (yellow triangles), almost stop (red squares) or even reverse (blue diamonds) the expansion of a freely falling BEC (purple circles). In addition, a concave matter-wave lens (dashed line) leads to an increase of expansion. Concave and convex lenses differ in delay time, as shown in the inset together with the dipole potential in time domain. (b) The experimental data (symbols) denotes the size of lensed ensembles after a total expansion time of 33.4 ms with pulses of various durations and optical powers. The delay time is 7.2 ms. The lines show numerical simulations obtained with a scaling approach. We indicate the minimum achievable and minimum observable size in the experiment due to atoms in the thermal background and aberrations of our matter-wave lenses and the detection system as a shaded area. Parameter sets of pulse duration and power which cause the matter-waves to focus during the detection (minima) are plotted in (c). For comparison, the black line indicates the relevant matter-wave lenses with a focal time $f_{\mathrm{DKC}} = 5.6$ ms predicted by the thin-lens equation (4) within a 1.5 ms interval.

of different shapes and refractive powers. The relevant focal times are obtained for any parameter set $(P, \tau, t_{\mathrm{del}})$ according to equation (6) with the results presented in figures 2(c) and 3(c).

Figure 4(a) shows ToF measurements, where we plot the size of BECs extracted from absorption images taken with multiple expansion times ranging from $t = 8$ to 34 ms (symbols). They are shown together with our theoretical predictions obtained with the scaling approach (lines). We utilize $\tau = 12.5$ μs long pulses to form matter-wave lenses of different focal times, which are either convex (dotted lines) or concave (dashed line). Convex and concave lenses differ in delay time, as becomes more visible in the inset of figure 4(a) together with the dipole potential for reference (shaded area). The selected delay times are $t_{\mathrm{del}} = 7.2$ ms and $t_{\mathrm{del}} = 6.8$ ms with $f_{\mathrm{DKC}}(7.2\ \mathrm{ms}) > 0$ and $f_{\mathrm{DKC}}(6.8\ \mathrm{ms}) < 0$, respectively.

In analogy to photonic waves in ray optics, the expansion of the matter waves is modified following the thin-lens equation (4), but in a time domain: optical pulses of various powers $P = (50, 120, 280)$ mW allow to reduce (yellow triangles), almost stop (red squares) or even reverse (blue diamonds) the expansion of the BEC. The related convex lenses cause a diverging ($f_{\mathrm{DKC}}(50\ \mathrm{mW}) = 18.3\ \mathrm{ms} > t_{\mathrm{del}}$), a nearly collimated ($f_{\mathrm{DKC}}(120\ \mathrm{mW}) = 7.6\ \mathrm{ms} \approx t_{\mathrm{del}}$) and a converging ($f_{\mathrm{DKC}}(280\ \mathrm{mW}) = 3.3\ \mathrm{ms} < t_{\mathrm{del}}$) matter wave. In contrast, the concave lens with a pulse of $P = 120$ mW leads to an increase of expansion, where $f_{\mathrm{DKC}}(120\ \mathrm{mW}) = -19.5$ ms causes a divergent matter wave.

We also examine if the employed lenses obey the thin-lens equation in a quantitative manner: in figure 4(b), we show the final BEC sizes of the ToF measurements after pulses of various durations $\tau = (6.3, 12.5, 25.0, 37.5, 62.5)$ μs with optical powers in the range of $P = 0$ to 600 mW (symbols). The delay time is $t_{\mathrm{del}} = 7.2$ ms. Numerical simulations with the scaling approach are shown as solid lines. The finite size limit of our experiment σ_{min} is indicated as a shaded area. For each pulse duration, the size of the BEC decreases, reaches a minimum and increases again for higher optical powers. Pulses that lead to the minimum BEC size relate to a matter-wave lens, which causes the matter wave to focus during the detection. The parameter sets of these pulses are plotted in figure 4(c) (symbols). The black line indicates the parameters of matter-wave lenses predicted by equation (4) with $t = t_{\mathrm{exp}} + t_{\mathrm{del}}$. The obtained focal time is $f_{\mathrm{DKC}} = 5.6$ ms. We find agreement with the experimental data within a 1.5 ms interval.

3.6. Hybrid matter-wave telescope

We realize a hybrid matter-wave telescope formed by a magnetic lens and an optical lens. Similar to the collimation of a divergent source with two lenses in a complementary arrangement, the magnetic and optical potentials of the atom-chip trap and ODT serve to collimate matter waves in two dimensions while magnifying the matter wave in one dimension. The parameters of the lensing potentials are shown in table 1.

After release from the magnetic trap, the BEC freely expands for $t_{\mathrm{del}} = 6.0$ ms before being exposed again to the magnetic fields of the atom chip. A $\tau = 300$ μs long box pulse of the magnetic potential

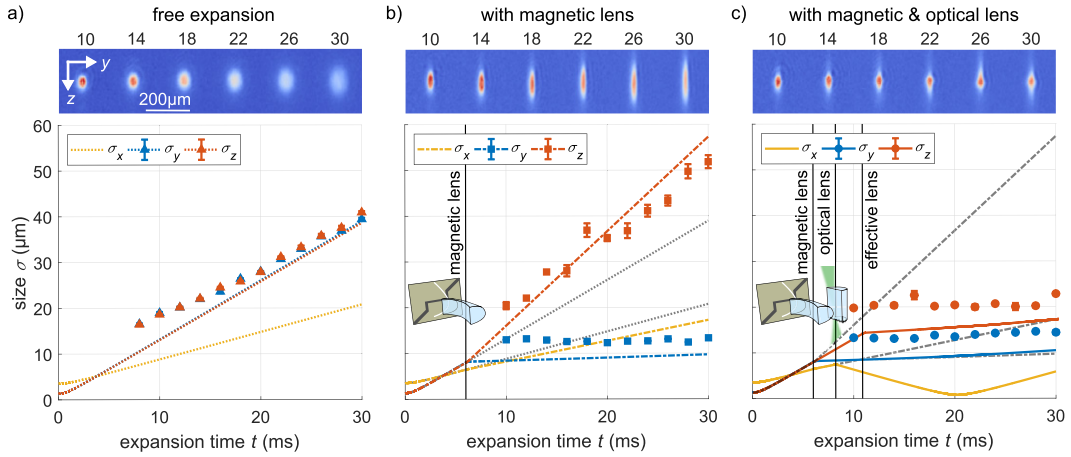

Figure 5. Hybrid matter-wave telescope. The magneto-optical lens system consists of two matter-wave lenses arranged in time. First, the magnetic lens diverges the matter wave along the z-axis. A subsequent optical lens then converges the matter-wave close to the point of collimation. This way, we form a Galilean-type telescope. ToF measurements of a BEC which (a) freely expands, and after exposure to either (b) the magnetic lens (delay time $t_{\mathrm{del}} = 6$ ms) or (c) the hybrid lens system (lens spacing $\delta t = 1.8$ ms) together with density profiles for selected expansion times. Black, vertical lines indicate the position of the lenses. The colored lines denote numerical simulations along multiple dimensions (yellow, blue, orange) obtained with a scaling approach in harmonic approximation. Preceding expansions are shown as gray lines for reference. Deviations result from the minimum observable and minimum achievable size in the experiment due to atoms in the thermal background and aberrations of matter-wave lenses and the detection system.

generates a matter-wave lens that is concave in one dimension and convex in the other ones. The effective trap frequencies are $(\omega_x, \omega_y, \omega_z)_{\mathrm{mag}} = 2\pi \cdot (44, 113, 90\mathrm{i})$ Hz, which we obtain from magnetic field simulations based on Biot–Savart's law with a simplified chip model. The corresponding focal times of the magnetic lens are $(f_x, f_y, f_z)_{\mathrm{mag}} = (+43.6, +6.6, -10.4)$ ms.

A second lens formed by a $P = 67$ mW, temporally shaped, Gaussian pulse of the dipole beam ($1/e^2$ width of $\tau = 25$ μs) completes the telescope. The optical potential with effective trap frequencies of $(\omega_x, \omega_y, \omega_z)_{\mathrm{opt}} = 2\pi \cdot (240, 3, 240)$ Hz generates a 2D cylindrical lens with focal times $(f_x, f_y, f_z)_{\mathrm{opt}} = (+6.9,\ 0, +6.9)$ ms. We choose a lens spacing of $\delta t = 1.8$ ms to match the COM position of the BEC with the center of the Gaussian beam, analog to the delay scans presented in figure 3.

Figure 5 shows ToF measurements of a BEC which (a) freely expands (triangles and dotted lines), and after exposure to either (b) the magnetic lens (squares and dashed lines) or (c) the hybrid lens system (circles and solid lines). Vertical lines indicate the position of the matter-wave lenses. We show density profiles for selected expansion times. Sizes of the BEC along the y- and z-axes are obtained by 2D Gaussian fits to the atomic density distributions, which we indicate as blue and orange symbols, respectively[8]. Simulations with the scaling approach including both the magnetic and optical potential in a harmonic approximation are shown as lines (yellow, blue, orange). Preceding expansions are shown as gray lines for reference.

Along the x-axis (yellow), both lenses are convex ($f_x > 0$) and the two-lens system causes the matter wave to refocus. This cannot be directly observed due to the detection limit within the experiment.

Along the y-axis (blue), the magnetic lens collimates the matter wave ($f_y \approx t_{\mathrm{del}}$). The subsequent optical lens does not affect the expansion on the examined timescale ($f_y \approx 0$). Nevertheless, we observe an increase in the asymptotic expansion imposed by the Gross–Pitaevskii interaction at high densities.

Along the z-axis (orange), the magnetic lens further increases the BEC's expansion ($f_z < 0$). The optical lens then converges the matter wave ($f_z > 0$) close to the point of collimation. This way, we form a one-dimensional, Galilean-type telescope able to magnify the matter wave, thus changing the aspect ratio of the ensemble.

The hybrid matter-wave telescope can be described by a single lens with a combined focal time analog to the concept of an effective focal length of a two-lens system

$$\frac{1}{f} = \frac{1}{f_{\mathrm{mag}}} + \frac{1}{f_{\mathrm{opt}}} - \frac{\delta t}{f_{\mathrm{mag}} \cdot f_{\mathrm{opt}}}, \tag{12}$$

where the position of this effective lens is $t = t_{\mathrm{del}} + \delta t \cdot (1 - f/f_{\mathrm{mag}})$. The numerical simulations of σ_z shown in figure 5(c) (orange) are derived with this combined lens of $f = 12.5$ ms instead of the two-lens system.

[8] We accommodate atoms inside the thermal background and lens aberrations of the magnetic lens with bimodal fits alongside the z-axis.

The scaling approach predicts the measured change of the ensemble's aspect ratio by a factor 1.4 within 16% agreement between simulations and experimental data. Deviations in absolute sizes result from the finite size limit of our experiment σ_{min} due to atoms in the thermal background and aberrations of the matter-wave lenses and the detection system.

4. Conclusion

Our combined atom-chip and dipole trap setup enables the flexible creation of matter-wave lenses employed in BECs. Atom lenses of various shapes and refractive powers can be engineered, e.g. through the timing, power and duration of the optical pulses of the single Gaussian beam. Lens systems formed by multiple atom lenses of different types then allow to manipulate both the dispersion and size of atomic matter waves.

The image formation can be predicted within a thin-lens formalism including anharmonicites attributed to the Gaussian beam, which we confirm experimentally. These findings prove this kind of experiment suitable to characterize arbitrary potentials by measuring the magnification of lensed matter waves. We can estimate an error on the measurement of the trap frequencies by acknowledging uncertainties in the timing of the lens δt_{del}, detection δt, lens duration $\delta\tau$ and size of the BEC $\delta\sigma$. From equation (7), we infer the relative error

$$\frac{\delta\omega_{\mathrm{DKC}}}{\omega_{\mathrm{DKC}}} = \frac{\delta\sigma}{\sigma'(t) \pm \sigma(t)} + \frac{\delta t}{t} + \frac{\delta\tau}{\tau} + \frac{\delta t_{\mathrm{del}}}{t_{\mathrm{del}}} \tag{13}$$

with equal impacts of the time observables. However, we see that larger changes in size $\sigma'(t) \pm \sigma(t)$ and extended expansion times t lower the overall error in terms of influence of $\delta\sigma$. To increase the resolution, the duration τ and timing t_{del} need to be short such that the thin-lens approximation is valid if $\omega_{\mathrm{DKC}}(t_{\mathrm{del}} \pm \tau) \approx \omega_{\mathrm{DKC}}(t_{\mathrm{del}})$ and lens aberrations are reduced if $\sigma(t_{\mathrm{del}}) \ll w_0$ (parabolic lens).

In addition, the scaling approach provides a good tool to model the evolution of BECs after release and manipulation in optical potentials including the influence of the finite trapping volume. We are able to match the asymptotic expansions with the experimental data. The model underestimates the absolute size close to the finite size limit σ_{min} and after refocusing of the matter waves, which we explain by the detection limit in our experiment, bimodal density distribution due to atoms in the thermal background and lens aberrations of the involved matter-wave lenses.

Lens systems, such as the matter-wave telescope presented in this work, allow to customize matter-wave packets in multiple dimensions. We anticipate lens systems with atom chips and crossed beam ODTs to reduce density-driven expansions towards unrivaled effective 3D temperatures.

Funding information

The presented work is supported by the German Space Agency (DLR) with funds provided by the Federal Ministry of Economic Affairs and Energy (BMWi) due to an enactment of the German Bundestag under Grant No. DLR 50WP1432 (QUANTUS-IV-MAIUS), 50WM1952 (QUANTUS-V-Fallturm), 50WP1700 (BECCAL), 50RK1957 (QGYRO), 50WM2055 (OPTIMO-2) Deutsches Zentrum für Luft-und Raumfahrt (DLR), the CRC 1227 DQmat within the projects A05 and B07, the CRC 1128 geo-Q within the projects A01 and A02, the QUEST-LFS, the Verein Deutscher Ingenieure (VDI) with funds provided by the Federal Ministry of Education and Research (BMBF) under Grant No. VDI 13N14838 (TAIOL).

We acknowledge financial support from 'Niedersächsisches Vorab' through the 'Quantum- and Nano-Metrology (QUANOMET)' initiative within the project QT3 and through 'Förderung von Wissenschaft und Technik in Forschung und Lehre' for the initial funding of research in the new DLR-SI Institute. Funded by the Deutsche Forschungsgemeinschaft (DFG, German Research Foundation) under Germany's Excellence Strategy – EXC-2123 QuantumFrontiers – 390837967. We acknowledge support by the DFG and the Open Access Publication Fund of Humboldt-Universität zu Berlin.

Acknowledgments

We would like to thank Thomas Flisgen for the collaboration on magnetic field simulations. We are grateful to Christian Vogt, Marian Woltmann and Sven Herrmann from the PRIMUS team for their support and helpful comments during the lab work. We would like to thank Victoria Henderson for proof-reading the manuscripts and we thank Sascha Vowe for fruitful discussions on the data analysis.

Data availability statement

The data that support the findings of this study are available upon reasonable request from the authors.

ORCID iDs

Simon Kanthak https://orcid.org/0000-0002-6576-8753
Martina Gebbe https://orcid.org/0000-0001-9591-9252
Matthias Gersemann https://orcid.org/0000-0003-1171-0166
Sven Abend https://orcid.org/0000-0001-9539-3780

References

[1] Adams C S, Sigel M and Mlynek J 1994 *Phys. Rep.* **240** 143–210
[2] Pfau T and Mlynek J 1994 *Phys. Bl.* **50** 45–50
[3] Szilagyi M 1988 *Electron and Ion Optics* (Berlin: Springer)
[4] Sears V F 1982 *Phys. Rep.* **82** 1–29
[5] Friedburg H 1951 *Z. Phys.* **130** 493–512
[6] Myrskog S H, Fox J K, Moon H S, Kim J B and Steinberg A M 2000 *Phys. Rev.* A **61** 053412
[7] Chu S, Bjorkholm J E, Ashkin A, Gordon J P and Hollberg L W 1986 *Opt. Lett.* **11** 73–5
[8] Sleator T, Pfau T, Balykin V and Mlynek J 1992 *Appl. Phys.* B **54** 375–9
[9] Morinaga M, Bouchoule I, Karam J-C and Salomon C 1999 *Phys. Rev. Lett.* **83** 4037–40
[10] McDonald G D, Kuhn C C N, Bennetts S, Debs J E, Hardman K S, Johnsson M, Close J D and Robins N P 2013 *Phys. Rev.* A **88** 053620
[11] Ramos R, Spierings D, Potnis S and Steinberg A M 2018 *Phys. Rev.* A **98** 023611
[12] Müntinga H *et al* 2013 *Phys. Rev. Lett.* **110** 093602
[13] Kovachy T, Hogan J M, Sugarbaker A, Dickerson S M, Donnelly C A, Overstreet C and Kasevich M A 2015 *Phys. Rev. Lett.* **114** 143004
[14] Smith D A, Arnold A S, Pritchard M J and Hughes I G 2008 *J. Phys. B: At. Mol. Opt. Phys.* **41** 125302
[15] Deppner C *et al* 2021 *Phys. Rev. Lett.* (accepted)
[16] Muniz S R, Jenkins S D, Kennedy T A B, Naik D S and Raman C 2006 *Opt. Express* **14** 8947–57
[17] Arndt M, Szriftgiser P, Dalibard J and Steane A M 1996 *Phys. Rev.* A **53** 3369–78
[18] Maréchal E, Guibal S, Bossennec J-L, Barbé R, Keller J-C and Gorceix O 1999 *Phys. Rev.* A **59** 4636–40
[19] Debs J E, Altin P A, Barter T H, Döring D, Dennis G R, McDonald G, Anderson R P, Close J D and Robins N P 2011 *Phys. Rev.* A **84** 033610
[20] Abend S *et al* 2016 *Phys. Rev. Lett.* **117** 203003
[21] Heine N, Matthias J, Sahelgozin M, Herr W, Abend S, Timmen L, Müller J and Rasel E M 2020 *Eur. Phys. J.* D **74** 174
[22] Ahlers H *et al* 2016 *Phys. Rev. Lett.* **116** 173601
[23] Hardman K S *et al* 2016 *Phys. Rev. Lett.* **117** 138501
[24] Eto Y, Ikeda H, Suzuki H, Hasegawa S, Tomiyama Y, Sekine S, Sadgrove M and Hirano T 2013 *Phys. Rev.* A **88** 031602
[25] Moan E R, Horne R A, Arpornthip T, Luo Z, Fallon A J, Berl S J and Sackett C A 2020 *Phys. Rev. Lett.* **124** 120403
[26] Leanhardt A E, Pasquini T A, Saba M, Schirotzek A, Shin Y, Kielpinski D, Pritchard D E and Ketterle W 2003 *Science* **301** 1513–5
[27] Inouye S, Andrews M R, Stenger J, Miesner H-J, Stamper-Kurn D M and Ketterle W 1998 *Nature* **392** 151–4
[28] Corgier R, Amri S, Herr W, Ahlers H, Rudolph J, Guéry-Odelin D, Rasel E M, Charron E and Gaaloul N 2018 *New J. Phys.* **20** 055002
[29] Ammann H and Christensen N 1997 *Phys. Rev. Lett.* **78** 2088–91
[30] Lachmann M D *et al* 2021 *Nat. Commun.* **12** 1317
[31] Gebbe M *et al* 2021 *Nat. Commun.* **12** 2544
[32] Aveline D C *et al* 2020 *Nature* **582** 193–7
[33] Frye K *et al* 2021 *EPJ Quantum Technol.* **8** 1
[34] van Zoest T *et al* 2010 *Science* **328** 1540–3
[35] Pérez-García V M, Michinel H, Cirac J I, Lewenstein M and Zoller P 1996 *Phys. Rev. Lett.* **77** 5320–3
[36] Pérez-García V M, Michinel H, Cirac J I, Lewenstein M and Zoller P 1997 *Phys. Rev.* A **56** 1424–32